



Contents lists available at ScienceDirect

# International Journal of Rock Mechanics & Mining Sciences

journal homepage: [www.elsevier.com/locate/ijrmms](http://www.elsevier.com/locate/ijrmms)

## Numerical simulation of thermal-hydrologic-mechanical-chemical processes in deformable, fractured porous media

Joshua Taron<sup>a,\*</sup>, Derek Elsworth<sup>a</sup>, Ki-Bok Min<sup>b</sup><sup>a</sup> Department of Energy and Mineral Engineering and Center for Geomechanics, Geofluids, and Geohazards (G3), Pennsylvania State University, University Park, Pennsylvania, USA<sup>b</sup> School of Civil, Environmental, and Mining Engineering, The University of Adelaide, SA, Australia

### ARTICLE INFO

#### Article history:

Received 7 August 2007

Received in revised form

28 October 2008

Accepted 20 January 2009

Available online 25 February 2009

#### Keywords:

THMC

Geothermal simulation

CO<sub>2</sub>

Fracture reactive transport

Reservoir permeability

Dual porosity

### ABSTRACT

A method is introduced to couple the thermal (T), hydrologic (H), and chemical precipitation/dissolution (C) capabilities of TOUGHREACT with the mechanical (M) framework of FLAC<sup>3D</sup> to examine THMC processes in deformable, fractured porous media. The combined influence of stress-driven asperity dissolution, thermal-hydro-mechanical asperity compaction/dilation, and mineral precipitation/dissolution alter the permeability of fractures during thermal, hydraulic, and chemical stimulation. Fracture and matrix are mechanically linked through linear, dual-porosity poroelasticity. Stress-dissolution effects are driven by augmented effective stresses incrementally defined at steady state with feedbacks to the transport system as a mass source, and to the mechanical system as an equivalent chemical strain. Porosity, permeability, stiffness, and chemical composition may be spatially heterogeneous and evolve with local temperature, effective stress and chemical potential. Changes in total stress generate undrained fluid pressure increments which are passed from the mechanical analysis to the transport logic with a correction to enforce conservation of fluid mass. Analytical comparisons confirm the ability of the model to represent the rapid, undrained response of the fluid-mechanical system to mechanical loading. We then focus on a full thermal loading/unloading cycle of a constrained fractured mass and follow irreversible alteration in *in-situ* stress and permeability resulting from both mechanical and chemical effects. A subsequent paper [Taron J, Elsworth D. Thermal-hydrologic-mechanical-chemical processes in the evolution of engineered geothermal reservoirs. Int J Rock Mech Min Sci 2009; this issue, doi:10.1016/j.ijrmms.2009.01.007] follows the evolution of mechanical and transport properties in an EGS reservoir, and outlines in greater detail the strength of coupling between THMC mechanisms.

© 2009 Elsevier Ltd. All rights reserved.

### 1. Introduction

It is well known that fractured rocks exhibit changes in mechanical compliance and hydraulic conductivity when subjected to thermal, hydraulic, mechanical, and chemical forces. In many engineering applications it is important to be able to predict the direction and magnitude of these changes. However, the interplay between temperature, effective stress, chemical potential, and fracture response is complex: it is not only influenced by anisotropic and spatially varying fracture properties, but also by fracture properties that are dynamic, and evolve with the dynamic nature of the applied forces.

The gapping or sealing of natural fractures has clear implications in reservoirs for the sequestration of CO<sub>2</sub> [2] and radioactive waste repositories [3], where the release of CO<sub>2</sub> or the redistribution of pore fluids around contained radioactive waste is a primary

concern. Volcanic environments are also impacted, as in the case of failing volcanic domes [4], where elevated fluid pressures may destabilize an existing volcanic pile. In other cases, such as petroleum or gas reservoirs, hot dry rock [5] or enhanced geothermal systems [6] (HDR/EGS), engineered stimulations may beneficially improve fluid circulation; a topic of significant interest since the majority of worldwide geothermal capacity is contained within low permeability rock masses [6,7].

Despite their importance, the competing influence of processes that degrade fluid conductivity in dominant fractures, such as thin-film pressure solution [8–10] and mineral precipitation, and those that enhance it, such as shear dilation [11,12], mineral dissolution [13–15], and strain energy driven free-face dissolution [9,16] have yet to be addressed at geologic scale. To examine these processes together, a link between chemical and mechanical behavior that maintains dependence on thermal and hydrologic changes is required, i.e., THMC coupling. And while several THM [3,17–20] and THC [14] coupling methodologies have been suggested, to the authors' knowledge no single numerical simulator has been introduced to examine THMC processes in a

\* Corresponding author. Tel.: +1 814 863 9733; fax: +1 814 865 3248.  
E-mail address: [jmt269@psu.edu](mailto:jmt269@psu.edu) (J. Taron).

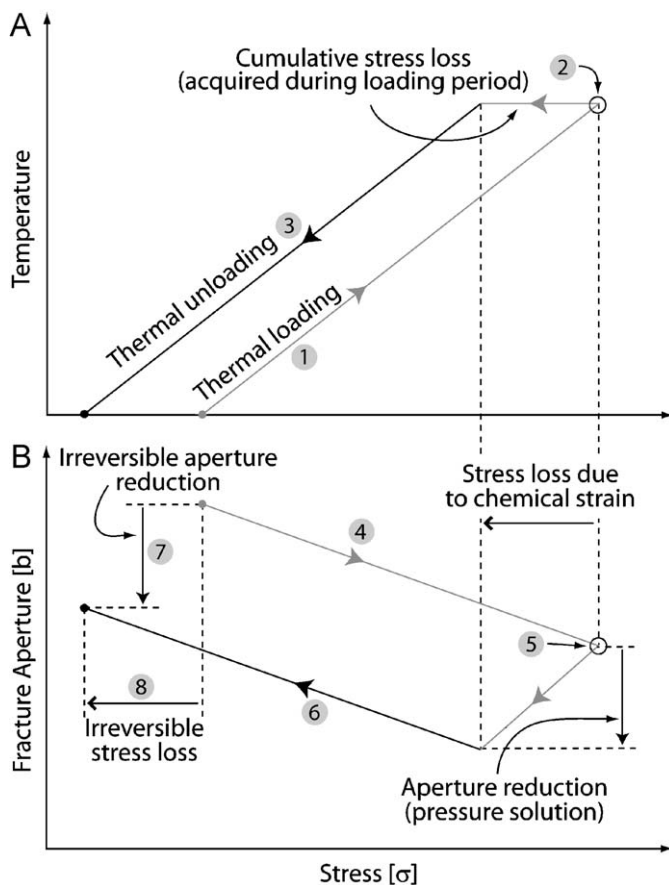


**Fig. 1.** Conceptual, behavioral trend of thermally loaded and fractured rock: (A) follow light gray line as (1) increasing temperature builds stress (partially reduced by elastic fracture strain). (2) Irreversible fracture strains reduce stress, which, for illustrative purpose, is applied at the end of loading (3). Thermal unloading follows the black line. (B) Follow gray temperature (stress) loading line (4) elastic reduction in fracture aperture (idealized as linear). Loading reaches maximum value (5). Aperture irreversibly closes (chemical strain) and causes corresponding drop in stress. Black (6) unloading line returns the system to its resting state for an (7) irreversible aperture reduction and (8) corresponding irreversible stress loss.

construct that is applicable to the broad variety of above-mentioned engineering applications.

Fig. 1 illustrates the potential error in excluding the chemical–mechanical link from numerical modeling. In the figure, we follow a complete cycle of thermal/stress loading in a chemically active fractured rock. During the loading/unloading cycle, reversible (elastic) and irreversible (chemical–mechanical: pressure solution or other) changes in aperture occur, with the ultimate result that after unloading, once the system has been returned to its initial background state, we see an irreversible aperture reduction, and a corresponding irreversible loss in the state of stress. These two occurrences (7 and 8 in Fig. 1) are the behaviors of primary interest, as they indicate a complete and potentially significant alteration of the resting system that cannot be represented without the inclusion of THMC processes.

## 2. Model capabilities

We now introduce and implement a method for coupling the multiphase, multi-component, non-isothermal thermodynamics, reactive transport, and chemical precipitation/dissolution capabilities of TOUGHREACT [14] with the mechanical framework of FLAC<sup>3D</sup> [21] to generate a coupled THMC simulator. This “modular” approach, first proposed by Settari [22] to couple

geomechanics with reservoir flow simulation, has some advantages over the development of a single coupled program. Modular approaches will typically be more rapid and less expensive to develop, although working within the framework of an existing code can sometimes lack the freedom that is inherent in “from scratch” code development. Additionally, as pointed out by Settari and Mourits [23], the modular construction allows for easier implementation of future advances in constitutive relationships or modeling structures (rather than modifying an entire coding structure), and the system can utilize highly sophisticated, rigorously validated existing codes developed at high cost. It can take many years for a new modeling structure to be validated by the research community, but in the case of TOUGHREACT and FLAC<sup>3D</sup>, each has been extensively scrutinized and each code is “qualified” for regulated programs, such as the US radioactive waste program.

Furthermore, single codes often simplify behavior beyond the principal scope of the analysis. For example, complex geomechanical codes may represent the flow system as only single phase, and complex reactive transport codes often incorporate mechanical response as invariant total stresses. Appropriate coupling enables the important subtleties of geomechanical response to be followed while maintaining complex fluid thermodynamics and reactive processes. Although development time is shortened in this modular approach, execution times are commonly extended, as neither code is optimized for the couplings, and data transfer must occur between the concurrently or sequentially executing codes. As suggested by Settari and Mourits [23] and Minkoff et al. [24], however, this may not always be the case, because in systems where geomechanics may be loosely coupled (not changing at a rapid pace) the geomechanics simulation may not need to be conducted very often, thus improving computational efficiency over fully coupled codes where mechanics are equilibrated at every fluid flow time step.

The coupled analysis that we present incorporates features unique to engineered geosystems, particularly those under elevated temperature and chemical potential, involving the undrained pressure response in a dual-porosity medium and stress-chemistry effects including the role of mechanically mediated chemical dissolution of bridging fracture asperities. FLAC<sup>3D</sup> is exercised purely in mechanical mode, where undrained fluid pressures may be evaluated (externally) from local total stresses. This undrained methodology allows calculation of the short-term build-up in fluid pressures that result from an instantaneous change in stress, provided we have knowledge of the compressibility of the pore fluids and the solid matrix. In this way, the complex thermodynamics of phase equilibria of multiphase water mixtures, and even multi-component mixtures (such as CO<sub>2</sub> and water), can be tracked in the pre-existing framework of TOUGHREACT. As TOUGHREACT has no use for compressibility, however, it is necessary to code this capability into the program or, as we have done, to insert a thermodynamic calculation into the external linking module (discussed later). For water mixtures, we utilize the 1997 International Association for the Properties of Water and Steam (IAPWS) steam table equations [25]. For CO<sub>2</sub> mixtures, an appropriate equation of state would be required, and we have not yet added this capability. If a system is unsaturated (such as in HDR/EGS), fluid compressibility is very large, and the undrained poroelastic equations approach their drained counterparts. Therefore, while our construct is tailored to saturated systems, drained systems are automatically accommodated.

FLAC<sup>3D</sup> is applied independent of time to accommodate the incremental equilibration of stresses for various mechanical constitutive relationships. TOUGHREACT performs time-dependent transport calculations, tracking thermodynamic relationships for temperature, phase equilibria, and pore pressure dissipation

together with aqueous chemical equilibrium and kinetic precipitation/dissolution in a dual-porosity medium. Under large thermal stresses, shear failure may be expected, and FLAC<sup>3D</sup> is capable of handling this with the constitutive theories of Mohr–Coulomb or Hoek–Brown. Plastic flow is also possible, although this would require consideration of permeability changes that occur during fracture shear and also fracture compression. This complexity is not addressed here, and will be the topic of a future paper.

### 3. Simulation logic

Simulation is executed within FLAC<sup>3D</sup>'s FISH programming language [21], where external operations by TOUGHREACT and the linking module are controlled. TOUGHREACT, an integral finite difference code [26], calculates all properties at the central coordinate of element volumes. In contrast, the first order finite difference program FLAC<sup>3D</sup>, with explicit temporal derivatives and a mixed discretization method that overlays constant strain-rate tetrahedral elements with the final zone elements (adding greater freedom in methods of plastic flow), utilizes properties of state ( $p, T$ ) at corner nodes and mechanical variables ( $\sigma, u$ ) at central coordinates. Correspondingly, state properties from central TOUGHREACT nodes are interpolated to connecting corner nodes of FLAC<sup>3D</sup>. Stress (not displacement) outputs from FLAC<sup>3D</sup> are used as the independent variable in constitutive relationships. The parsing of stresses to TOUGHREACT is direct, as they are calculated centrally within the node-centered blocks of FLAC<sup>3D</sup> (in spatial agreement with TOUGHREACT).

In its current construction, the codes iterate upon the same numerical grid. This structure, however, is not required. As pointed out by Minkoff et al. [24], un-matched meshes are one benefit to a modular code. For example [24], it may be desirable to conduct flow simulations upon a reservoir area impacted by fluid injection and withdrawal only, while the mechanical grid may include the reservoir area in addition to all overburden up to the ground surface. Neither must the overlapping simulation areas utilize identical grid spacing, such that it may be desirable to refine the fluid flow mesh to capture some complex physics in a specific area, without adapting the mechanical mesh to agree. It is only required that interpolation of data accommodate the differences in mesh extent and geometry.

Sequential execution of the two programs is linked by a separate code capable of parsing data outputs from each primary simulator as input to the companion. This separate code is referred to as the "interpolation module". The module is a Fortran 90 executable, and maintains access to data outputs from TOUGHREACT and FLAC<sup>3D</sup>. In addition to data interpolation, this module executes constitutive relationships including permeability evolution, dual-porosity poroelastic response to stress, and thermodynamically controlled fluid compressibility.

All transient calculations take place within TOUGHREACT, and it is here that the time step is controlled for conditions of fluid velocity, grid size, and reaction rates. Additionally, there is a secondary (explicit) time step that controls how often stress is corrected to changes in fluid pressure (for what length of time TOUGHREACT conducts a flow simulation before allowing stress equilibration in FLAC<sup>3D</sup>). This frequency is controlled in the interpolation module. If the magnitude of stress change in the system over one time step is beneath a pre-determined tolerance, the frequency is decreased (if stress is not changing, mechanical re-equilibration is unnecessary), and vice versa for an upper tolerance. Coupling is explicit and constitutive calculations are performed once per iteration (assuming constant constitutive values throughout a fluid flow time step), requiring sufficiently

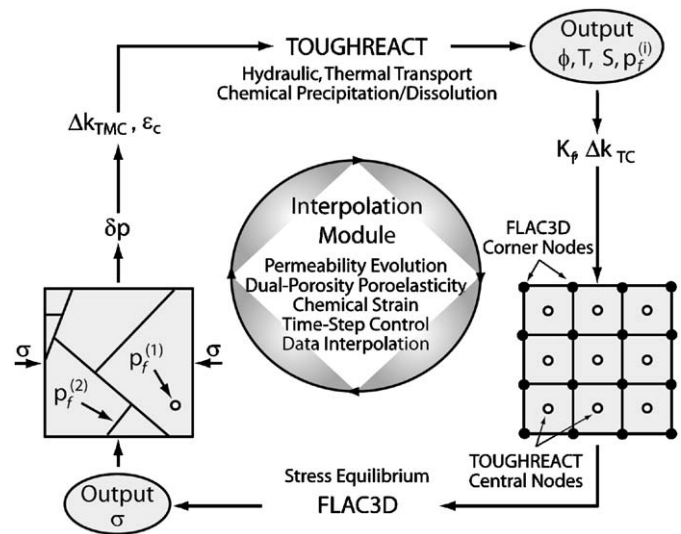


Fig. 2. Coupling relationship between TOUGHREACT, FLAC<sup>3D</sup>, and the interpolation module.

small time steps relative to the rapidity of change in the system. The validity of utilizing such a methodology is discussed in later sections to provide insight into this explicit time step.

The coupling cycle is shown in Fig. 2, and is comparable to the loose coupling, modular structure of Minkoff et al. [24] and Rutqvist et al. [3]. Simulation begins with equilibration of temperature ( $T$ ) and pore fluid pressure ( $p_f$ ) in TOUGHREACT, where porosity ( $\phi$ ) changes due to mineral precipitation/dissolution and liquid saturation ( $S$ ) are also obtained. Constitutive relationships in the interpolation module transform these outputs into fluid bulk modulus ( $K_f$ ), as obtained from IAPWS steam table equations, and permeability change due to mineral behavior ( $\Delta k_{TC}$ ). The TOUGHREACT central node data ( $p_f, T$ ) are then interpolated to corner node information as input to FLAC<sup>3D</sup>. After stress equilibration in FLAC<sup>3D</sup>, the interpolation module uses stress outputs within a dual-porosity framework, consisting of matrix ( $p_f^{(1)}$ ) and fracture ( $p_f^{(2)}$ ) pore fluid pressures, to obtain the pressure response to the new stress field via domain (*matrix, fracture*) and state ( $p, T$ ) specific Skempton coefficients. Effective stress is then used to obtain the permeability change due to pressure solution type behavior ( $\Delta k_{TMC}$ ) while chemical strain ( $\epsilon_c$ ) is accommodated in the stress field (discussed later). Parameters then re-enter TOUGHREACT for the next time step.

### 4. Governing equations

The physical system of interest is modeled herein as a multi-continuum, fully or partially saturated fracture/matrix system with direct communication between the domains. Local thermal equilibrium is assumed between the fluid and solid (at a single point in continuum space, the fluid and solid exhibit the same temperature), but not between separate fracture and matrix domains. From this framework, a differential of pressure and temperature may develop between the fracture and matrix, with properties of pressure and temperature dissipation influencing the rapidity of transfer from local changes in the fracture system into the surrounding matrix blocks, and vice versa. As such, the multi-continuum distinction is fully maintained within the numerically represented THC system, while local continuity of stress requires equilibrium of stresses between fracture and matrix, which is then represented within the single continuum framework of FLAC<sup>3D</sup>. For this transition, physical characteristics

are delegated based upon dual-porosity poroelastic theory [27–31]. The governing balance equations and their constitutive counterparts are discussed below.

#### 4.1. Conservation of momentum—solid

Mechanical equilibrium of the solid phase is governed by the balance of linear momentum,

$$\sigma_{ij,j} + b_i = \rho \dot{v}_i, \quad (1)$$

where  $b_i$  are the body forces per unit volume,  $\dot{v}_i$  are the material time derivatives of velocities, and  $\sigma_{ij,j}$  represents the divergence of the transpose of the Cauchy stress tensor. In an iterative formulation, for static equilibrium of the medium, the momentum balance becomes the common force equilibrium relation

$$\sigma_{ij,j} = -b_i. \quad (2)$$

The resulting unknowns can be related to each other through any of several elastic or plastic constitutive relationships. We begin with the case of an isotropic, elastic solid, thus introducing the stress/strain constitutive relationship for a medium with two distinct porosities (see dual-porosity discussion below), including the effects of pore fluid pressure,  $p$ , and temperature,  $T$  (a combined equation utilizing constitutive poroelasticity (e.g. [32], Eq. 7.42), with thermoelastic response, and utilizing two distinct pore fluid pressures as in Wilson and Aifantis [27]),

$$\sigma_{ij} = 2G\varepsilon_{ij} + \frac{2G\nu}{1-2\nu}\varepsilon_{kk}\delta_{ij} - (\alpha_p^{(1)}p + \alpha_p^{(2)}p)\delta_{ij} - \alpha_T T\delta_{ij}, \quad (3)$$

where  $G$  is the shear modulus,  $\nu$  is the Poisson ratio,  $\alpha_p^{(i)}$  and  $\alpha_T$  are the coupling coefficients for fluid and thermal effects for the <sup>(1)</sup> fracture and <sup>(2)</sup> matrix,  $\delta_{ij}$  is the Kronecker delta, and the linearized (“small”) strains are defined as the symmetric part of the displacement gradient  $u_{i,j}$ , i.e.,

$$\varepsilon_{ij} = \frac{1}{2}(u_{i,j} + u_{j,i}). \quad (4)$$

Inserting Eq. (4) into Eq. (3) and the result into the equilibrium equation, Eq. (2), yields the Navier equation for the displacements,  $u$

$$G\nabla u_i + \frac{G}{1-2\nu}u_{k,ki} = (\alpha_p^{(1)}p_{,i} + \alpha_p^{(2)}p_{,i}) + \alpha_T T_{,i} - b_i, \quad (5)$$

#### 4.2. Conservation of momentum, mass, and energy—fluid

Fluid, aqueous species, and energy are transported through the system as defined by their respective mass and energy balances. The master equation for these processes is given in integral form as

$$\frac{d}{dt} \int_V M_\kappa dV = \int_\Gamma \mathbf{F}_\kappa \cdot \mathbf{n} + \int_V q_\kappa dV, \quad (6)$$

where the left-hand side represents the rate of accumulation of the conserved quantity ( $M_\kappa$  is mass of fluid, mineral mass, or energy density) resulting from the arrival of the fluxes  $\mathbf{F}_\kappa$ , (of fluid, mass, or energy) across the boundary,  $\Gamma$ , and complemented by volume sources,  $q_\kappa$ , distributed over the nominal element volume,  $V$ , for each component,  $\kappa$  (gas, liquid, advected species, or heat). In this discussion we have adopted (for clarity of coefficients) standard tensor notation, where bold values represent first or second order tensors. Eq. (6) may be transformed into its common PDE counterpart through use of the divergence theorem

$$\frac{\partial M_\kappa}{\partial t} = -\nabla \cdot \mathbf{F}_\kappa + q_\kappa, \quad (7)$$

where the mass, flux, and source terms must then be independently determined for a given system.

Mass, or energy density,  $M_\kappa$ , in Eq. (7) is defined for each component,  $\kappa$ , as the summation of the various contributions to the component across all phases (subscripted  $l, g, s$  for liquid, gas, or solid) as

$$M_\kappa = \phi S_l \rho_l X_l + \phi S_g \rho_g X_g + (1 - \phi) \rho_s X_s, \quad (8)$$

where  $S$  is phase saturation,  $\rho$  is density (or species concentration),  $\phi$  is porosity, and  $X_{s,l,g}$  is mass fraction (or internal energy). Simplification then occurs for each calculation. The third term disappears for fluid mass calculations (no solid phase present), while the second and third terms are excluded from aqueous species mass (species may be present within the liquid medium, but not solid or gaseous).

Fluxes,  $\mathbf{F}$ , in Eq. (7) are given by the summation across phases ( $\beta = l, g$ ) of the advective and diffusive terms as

$$\mathbf{F} = \sum_{\beta=l,g} \left( -X_\beta \rho_\beta \frac{\mathbf{k}k'_\beta}{\mu_\beta} (\nabla p_\beta - \rho_\beta \mathbf{g}) \right) - \lambda_\beta \nabla C, \quad (9)$$

where the first term represents the contribution of advection through consideration of the multiphase extension of Darcy's law for relative permeability,  $k'$ , intrinsic permeability vector,  $\mathbf{k}$ , dynamic viscosity,  $\mu$ , and, as before,  $\rho$  is density of fluid (or concentration of species) and  $X$  is mass fraction for fluid transport, specific enthalpy for heat flow, or unity for chemical calculations. The second term represents diffusive transport as governed by the laws of Fick and Fourier, and introduces conductivity,  $\lambda_\beta$ , and gradient (of temperature or concentration),  $\nabla C$ . This last diffusive term is only present when calculating the flux of temperature or concentration, and therefore disappears when calculating pure liquid flux. For heat flow calculations,  $\lambda_\beta$  is thermal conductivity, while for chemical flux  $\lambda_\beta = \rho_\beta \tau \phi S_\beta D_\beta$  with tortuosity,  $\tau$ , and diffusion coefficient,  $D_\beta$ . Note that a hydrodynamic dispersion concept is not utilized in the classic Fickian sense. Instead, TOUGHREACT utilizes the interaction of regions with differing velocities (fracture and matrix in a dual-porosity construct) to induce solute mixing [33]. In the case of mineral mass, the flux term disappears (colloid transport is not considered).

The source term,  $q_\kappa$ , in Eq. (7) may be comprised of an injection or withdrawal source or as an increase in species concentration (or mineral mass) due to dissolution (or precipitation). A thermal source may also arise due to a release of energy during chemical reactions. This last case is not currently considered. Sources of aqueous species and/or mineral mass are discussed in the following.

#### 4.3. Chemical precipitation/dissolution

A generalized rate law for precipitation/dissolution of a mineral,  $m$ , is [34,35],

$$r_m = \text{sgn}(\log(Q_m/K_m^e)) k_m^c A_m f(a_i) \left| 1 - \left( \frac{Q_m}{K_m^e} \right)^\phi \right|^n, \quad (10)$$

where  $k^c$  is the rate constant,  $A$  is the specific mineral reactive surface area per kg of H<sub>2</sub>O,  $K^e$  is the mineral/water equilibrium constant, and  $Q$  is the ion activity product. The function  $f(a_i)$  represents some (inhibiting or catalyzing) dependence on the activities of individual ions in solution such as H<sup>+</sup> and OH<sup>-</sup> [36], and  $\text{sgn}(Q_m/K_m^e)$  provides a direction of reaction: positive for supersaturated precipitation. The exponential parameters,  $\phi$  and  $n$ , indicate an experimental order of reaction, commonly assumed to be unity. An additional term (multiplied by Eq. (10)) may also be introduced to represent the dependency of reactive surface area on liquid saturation [33]. Dependency of the rate constant

may be handled, to a reasonable approximation [37], via the Arrhenius expression,

$$k^c = k_{25}^c \exp\left(-\frac{E_a}{R_u}\left(\frac{1}{T} - \frac{1}{298.15}\right)\right), \quad (11)$$

for the rate constant at 25 °C,  $k_{25}^c$ , activation energy,  $E_a$ , and gas constant,  $R_u$ .

In the case of amorphous silica an alternate expression may be used following [38], where the precipitation rates reported in [39] were observed to underestimate behavior in geothermal systems. This new rate law, based upon experimental data for more complex geothermal fluids, becomes, in a form modified in [40] to approach zero as  $Q/K$  approaches one (i.e., as the system approaches equilibrium)

$$r_m = \text{sgn}(\log(Q_m/K_m^e))k_m A_m f(a_i) \left| \left(\frac{Q_m}{K_m^e}\right)^\mu - \left(\frac{K_m^e}{Q_m}\right)^{2\mu} \right|^n. \quad (12)$$

These are the formulations utilized in TOUGHREACT. Reactions between aqueous species (homogeneous reactions) are assumed to be at local equilibrium, and therefore governed by the relationship between the concentrations of basis (primary) species and their activities, partitioned by the stoichiometric coefficients. This relationship is termed the law of mass action (e.g. [34]). The assumption of local equilibrium greatly reduces the number of chemical unknowns and ODEs (between primary and secondary species), and is accurate to the extent that the true reaction rates outpace the rate of fluid transport in a given system. This is a correct assumption for most aqueous species [34] (and flow systems), but less so for slower redox reactions [33,34]. In TOUGHREACT, species activities are obtained from an extended Debye–Hückel equation with parameters taken from [41].

### 5. Deformable dual-porosity material

To represent the pressure loading of a fully or nearly liquid saturated system (particularly at high temperature and pressure and with multi-component liquids) coupling of the above formulation requires the undrained (instantaneous) response of pore fluid pressure to mechanical loading in both the fracture and matrix domains. Hydrologic considerations allow a timed pressure-dissipation response throughout the fracture dominated fluid system and between the fracture/matrix companionship following undrained loading.

Classically, a dual-porosity material is represented as a porous matrix partitioned into blocks by a mutually orthogonal fracture network [42,43]. In this scenario, permeability is much higher within the fracture network, thus allowing global flow to occur primarily through the fractures, while the vast majority of storage occurs within the higher porosity matrix (due to its larger global fraction of the medium). Interchange of fluid and heat between fractures and matrix, so-called “interporosity flow”, is driven by pressure or temperature gradients between the two domains.

Expansion of this classic two-domain interaction into “multi-interacting continua” [44,45] allows the gradual evolution of gradients between fracture and matrix through the existence of one or more intermediate continua placed, mathematically, some linear distance from the fracture domain. This development has allowed for numerical approximations to more accurately represent the slow invasion of locally (to the fracture) altered pressures and temperatures deeply into the matrix blocks, and introduced dispersive mixing that arises at the interface of zones with differing fluid velocities. While this multi-continuum methodology may be adopted in TOUGHREACT to represent dual-permeability fluid transport with uniformly constant stress fields in

time, we do not seek such an expansion with respect to a flow-deformation response [46]. As such, a dual-porosity framework with two interacting continua (fracture and matrix) is utilized in this study, while a compatible poroelastic theory carries this behavior into the mechanical domain.

#### 5.1. Fluid pressure response

Extension of Biot’s poroelastic theory [47–50] to a dual-porosity framework has been previously addressed [27–31, 46,51]. The methodologies presented in these works provide an adequate framework for the phenomenological representation of poroelastic coefficients capable of describing flow-deformation response in such a medium.

Continuity of fluid mass is represented in a compressible media as,

$$\frac{\partial \zeta}{\partial t} + \nabla \cdot \mathbf{F} = 0, \quad (13)$$

where  $\zeta$  is the increment of fluid content as in [52], and comprises the relative motion between fluid and solid. Inserting Darcy’s law for the flux term yields

$$\frac{\partial \zeta}{\partial t} - \frac{k}{\mu} \nabla^2 p = q. \quad (14)$$

Biot’s [48] linear-poroelastic constitutive equivalence, for volumetric strain,  $e$ , is

$$\begin{pmatrix} e \\ \zeta \end{pmatrix} = \begin{pmatrix} 1 & 1 \\ K & H \\ 1 & 1 \\ H & R \end{pmatrix} \begin{pmatrix} \sigma \\ p \end{pmatrix}, \quad (15)$$

where the coefficients  $1/K$ ,  $1/H$ , and  $1/R$  are the bulk drained compressibility, poroelastic expansion, and specific storage, respectively. Substituting

$$B \equiv -\frac{\delta p}{\delta \sigma} \Big|_{\zeta=0} = \frac{R}{H}, \quad (16)$$

for the Skempton coefficient,  $\alpha \equiv K/H$ , for the Biot–Willis coefficient and

$$\frac{1}{R} \equiv \frac{\delta \zeta}{\delta p} \Big|_{\sigma=0} = \frac{\alpha}{KB}, \quad (17)$$

for the specific storage, condensing Eq. (15) to relate fluid content to strain, and substituting its time derivative in Eq. (14), establishes the flow condition for a single-porosity medium with no fluid sources

$$\frac{\alpha}{BK_u} \dot{p} + \alpha \dot{e} = \frac{k}{\mu} \nabla^2 p, \quad (18)$$

where we have utilized the relationship for undrained bulk modulus,

$$K_u \equiv \frac{\delta \sigma}{\delta e} \Big|_{\zeta=0} = \frac{K}{1 - \alpha B}. \quad (19)$$

Extending to a dual-porosity medium, we follow the same procedure leading to the dual-porosity form of Eq. (5), where Eq. (18) is modified to exhibit two separate fluid pressures (for fracture and matrix) with flow between them governed by, in its simplest form, an instantaneous pressure differential,  $\Delta p = (p_1 - p_2)$  [42], to obtain two continuity relationships [28],

$$\frac{k^{(i)}}{\mu} \nabla^2 p^{(i)} = \frac{\alpha^{(i)}}{K^{(i)}B^{(i)}} \dot{p}^{(i)} + \alpha^{(i)} \dot{e} + (-1)^i \gamma \Delta p, \quad (20)$$

where  $i$  is not a repetitive index, but represents the existence of two separate equations for the matrix ( $i = 1$ ) and fracture ( $i = 2$ ),

and  $\gamma$  is the cross coupling coefficient for flow exchange between the two domains [53]. Eq. (20) states that the divergence of fluid flux for a given control volume must equal the rate of accumulation within that volume, and is thus a statement of mass conservation.

### 5.2. Dual-porosity load response

The general linear relation between strain, increment of fluid content, total stress ( $\sigma$ ), and pore fluid pressure ( $p$ ), simply extends Eq. (15) to allow, again, for two separate fluid pressures [31]

$$\begin{pmatrix} \delta e \\ -\delta\zeta^{(1)} \\ -\delta\zeta^{(2)} \end{pmatrix} = \begin{pmatrix} c_{11}c_{12}c_{13} \\ c_{21}c_{22}c_{23} \\ c_{31}c_{32}c_{33} \end{pmatrix} \begin{pmatrix} -\delta\sigma \\ -\delta p^{(1)} \\ -\delta p^{(2)} \end{pmatrix}, \quad (21)$$

where the superscripts refer to the (1) matrix and (2) fracture domains. The single porosity coefficients of Biot are no longer applicable, and are replaced by the unknown coupling coefficients,  $c_{ij}$ , that may be designated via a phenomenological deconstruction similar to that of Biot and Willis [52]. The coefficient matrix can be shown to be symmetric [31] by the Betti reciprocal theorem. Performing manipulations of the above equation through isolation of independent components (i.e. long-time versus short-time limits) allows determination of the central coefficients (see detailed procedure in [31,30]).

Herein we assume that  $c_{23} = c_{32} = 0$  [31], which differs slightly from the procedure of [27,28,30]. Examination of Eq. (21) shows that this assumption implies the following: an undrained application of stress that influences a change in fluid content for the fracture domain does so through modification of fracture fluid pressure, and does not influence that of the matrix. The reverse is also true, with the overall implication being, see discussion in Berryman and Wang [31], that in the undrained limit the matrix and fracture domains are completely separate. This can be considered a justification for a dual-porosity approach [31].

In our analysis, the purpose of dual-porosity elasticity is to attain Skempton coefficients representing both the fracture and matrix domains

$$\begin{aligned} \delta p^{(1)} &= B^{(1)}\delta\sigma = -\frac{c_{12}}{c_{22}}\delta\sigma \\ \delta p^{(2)} &= B^{(2)}\delta\sigma = -\frac{c_{13}}{c_{33}}\delta\sigma, \end{aligned} \quad (22)$$

which represent the undrained ( $\delta\zeta = 0$ ) build in pore fluid pressure in each domain for a given change in stress as provided by FLAC<sup>3D</sup>. Relationships to calculate these two Skempton coefficients are provided in Table 2 of [31]. For this procedure, we choose as the known coefficients  $K^{(1)}$ ,  $K$ ,  $K_s^{(1)}$ , and  $K_f$ , where  $K_s$  is the solid grain modulus (in a microhomogeneous medium [54]) and the fluid bulk modulus,

$$\frac{1}{K_f} \equiv \frac{1}{V} \frac{\delta V}{\delta p} \Big|_T, \quad (23)$$

is calculated in the interpolation module as a function of position, temperature, and pressure utilizing the IAPWS steam table equations [25]. For a complete reconstruction of the individual relations required to represent the dual-porosity poroelastic response, refer to [31,51].

### 5.3. Effect on the global mass balance

Injection of fluid mass into TOUGHREACT in the form of fluid pressure violates conservation of mass by an amount proportional to the compressibility of the local fluids. A change in pressure by

this procedure necessitates a change in local fluid volume, and therefore appearing or disappearing mass. However, when the local element is fully saturated, a stiff fluid will not significantly respond (volumetrically) to stress induced pressure changes, while for unsaturated media even a significant volumetric response will not in general dictate a noticeable change in mass. Nonetheless, we err on the side of safety and correct for this discrepancy with a recast of Eq. (23),

$$dV = \frac{1}{K_f} V dp \Big|_T, \quad (24)$$

which indicates the volume (or mass) error due to an increase in pressure,  $dp$  (at a given temperature). To correct for potential mass loss, we alter elemental volumes (physically reduce the volume of the mesh element) within TOUGHREACT by this amount (in an integral finite difference formulation, this does not require the alteration of geometric coordinates). In our simulations, including both single and multiphase flow with water/steam phase changes occurring, we have not detected total system mass losses greater than ~0.01% of total system mass.

## 6. Undrained fluid/mechanical response

We now examine the error that our formulation introduces to the fluid-mechanical coupling. Excluding constitutive approximations, error may be introduced into the coupling procedure as it has been described up to this point in two primary ways: explicit time step size, and the equilibration step between a stress change and its undrained pressure response (Fig. 3).

The first is a direct byproduct of explicit coupling, inasmuch as an increase in time step (length of the TOUGHREACT fluid step between each mechanical equilibration), allows a greater amount of fluid pressure to diffuse between each mechanical equilibration, introducing error proportional to the fluid diffusivity and inversely proportional to the rate of mechanical change (not the amount of mechanical change per timestep,  $d\sigma$ , which implies proportionality to error, but the rate of change per unit time ( $d\sigma/dt$ ), implying inverse proportionality).

The second form of error, shown in Fig. 3, is due to the nature of the undrained pressure response, which may not be fully accommodated by a single stress equilibrium step. In other words, at a given time step a fixed pressure field enters FLAC<sup>3D</sup> and is accommodated by a calculated stress distribution. This stress distribution induces a modification of the previously fixed pressure field, and this new pressure field may, in turn, produce a redistribution of the stress field whether or not any fluid is allowed to diffuse (within TOUGHREACT). A number of steps may

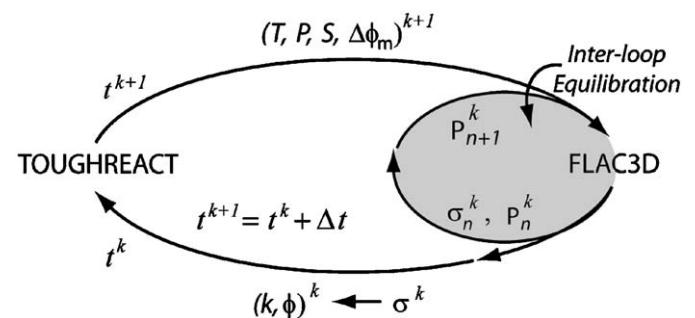


Fig. 3. Relationship between coupling methodologies. Interior looping may occur over  $n$  steps (at fixed time,  $t = t^k$ ) to equilibrate the response of stress to an undrained increase in pressure. Alternatively, this inter-looping may be excluded in favor of a “leapfrog” method, where a single stress equilibration (run of FLAC<sup>3D</sup>) is conducted per time step.

be required to find the true equilibrium magnitude of stress and pressure, which tends to asymptote at a value higher than is suggested by a single equilibration step. This is not necessarily a Mandel-Cryer type effect [55,56], which is a real occurrence and would require the action of a diffusing fluid pressure and redistribution of stresses around the diffusing magnitudes (although the behavior is comparable). The case where FLAC<sup>3D</sup> is run once per explicit time step (single equilibration step) is referred to herein as the “leapfrog method” (Fig. 3). Each of these possible error sources (<sup>1</sup>explicit time step and <sup>2</sup>leapfrog versus  $p = \sigma$  iteration) requires further examination, which consequently leads to validation of the undrained fluid-mechanical coupling.

6.1. Fluid-mechanical couple: instantaneous loading

In one dimension, we may examine the accuracy of the fluid-mechanical coupling in comparison to the classical fluid diffusion equation of hydrogeology (e.g. [57]),

$$\frac{\partial p}{\partial t} - c_f \frac{\partial^2 p}{\partial z^2} = 0, \tag{25}$$

which is a specific poroelastic result of Eqs. (14) and (15) restricted to a one-dimensional column of soil (or rock) under constant applied vertical stress [58], and gives its form to the analytical solution for heat flow [59, p. 96]

$$p(z, t) = \frac{4p_0}{\pi} \sum_{m=0}^{\infty} \frac{1}{2m+1} \exp(-\Psi^2 c_f t) \sin(\Psi z), \tag{26}$$

where  $\Psi = (2m + 1)\pi/2L$ , and  $p_0 = B^{(v)}\sigma_0$  is the initial undrained pressure response to the applied vertical stress ( $\sigma_0$ ). The one-dimensional Skempton coefficient (“loading efficiency” in [58]) is given by

$$B^{(v)} = -\frac{B(1 + \nu_u)}{3(1 - \nu_u)}, \tag{27}$$

for the Skempton coefficient,  $B$ , and undrained Poisson ratio,  $\nu_u$ . This is the canonical consolidation problem of a one-dimensional column of soil subjected to a constant vertical stress applied at  $t = 0^+$  to the top of the column, with fluid pressure allowed to drain freely from the point of applied stress. A similar solution is available for column displacement  $u$  (e.g. [48,58]),

$$\frac{\partial^2 u}{\partial z^2} = c_m \frac{\partial p}{\partial z}, \tag{28}$$

for Geertsma’s [60] uniaxial expansion coefficient (consolidation coefficient),  $c_m \equiv \alpha/K^{(v)}$ , with uniaxial bulk modulus,  $K^{(v)} = K+4G/3$ . Under the same boundary conditions as above, the analytical solution is [58]

$$\Delta u(z, t) = c_m p_0 \left[ (L - z) - \frac{8L}{\pi^2} \sum_{m=0}^{\infty} \frac{1}{(2m + 1)^2} \exp(-\Psi^2 c_f t) \cos(\Psi z) \right], \tag{29}$$

with definitions the same as for Eq. (26), and the instantaneous displacement at the time of stress application  $u(z, 0^+) = \sigma_0(L-z)/K_u^{(v)}$ , for the undrained uniaxial bulk modulus,

$$K_u^{(v)} = \frac{K_u(1 + \nu_u)}{3(1 - \nu_u)}. \tag{30}$$

All undrained parameters approach their drained counterparts as fluid compressibility becomes large, or fluid saturation approaches zero.

Results of a TOUGHREACT-FLAC<sup>3D</sup> simulation mimicking these boundary conditions are presented against these analytical solutions in Fig. 4. A column of porous rock ( $E = 13$  GPa,

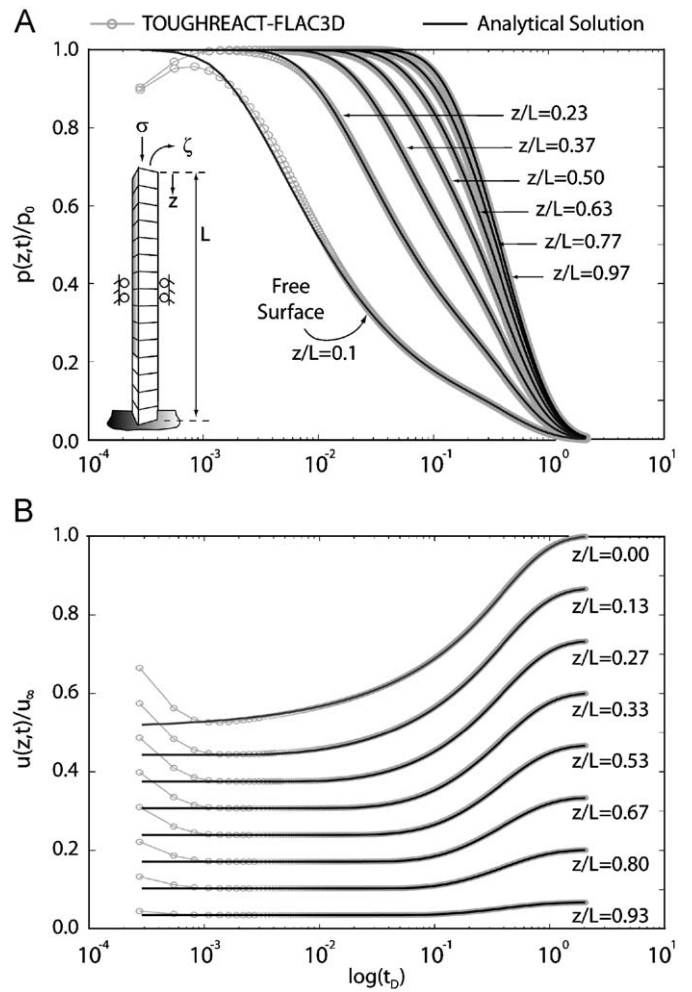


Fig. 4. Comparison of TOUGHREACT-FLAC<sup>3D</sup> fluid-mechanical coupling simulation versus analytical results in one dimension: (A) normalized ( $p_0 = p(z,0) = B^{(v)}\sigma_0$ ) pressure diffusion response versus diffusive time ( $t_D = ct/L^2$ ); (B) normalized ( $u_\infty = u(0, \infty) = \sigma_0 L/K^{(v)}$ ) displacement response versus diffusive time.

$\nu = 0.22$ ) with displacements constrained laterally and pore pressure initially zero, is subjected to an applied vertical load,  $\sigma_0 = 50$  MPa, at  $t = 0^+$ , and pressure is allowed to drain freely from the top of the column only. Time step was chosen large enough to illustrate the error incorporated in very early times (near the time of undrained loading) due to the leapfrog method of simulation (Fig. 3).

Pressure builds up (and elastic displacement decreases) in the early stages as the model cycles between stress equilibration and undrained pressure response (leapfrog artifact). Following the instantaneous loading period (50 MPa applied over one time step) numerical results overlay nearly identically the analytical solution as pressure diffuses and stress accommodates the pressure reduction. A slightly greater error occurs at points nearest the free draining surface (left-most curve in Fig. 4A) due to the explicit time step size, where a greater rate of fluid diffusion allows the fluid to move greater distances before being accommodated by a mechanical response.

6.2. Fluid-mechanical couple: constant loading rate

In light of Fig. 4, it is of interest to examine more precisely the error that arises while the sample is being loaded. To do so, we wish to utilize the same geometry, but apply the load gradually over a finite loading period at a given loading rate,  $d\sigma_0/dt$  (rate of

increase of applied load at the top of the column per unit time). Here, we maintain the one-dimensional form, but alter the governing diffusion equation (25) to accommodate a constant loading rate [58]:

$$\frac{1}{c_f} \frac{\partial p}{\partial t} - \frac{\partial^2 p}{\partial z^2} = \frac{c_m \mu}{k} \frac{d\sigma_0}{dt}, \quad (31)$$

with the series solution adjusted so that, as above, the free draining boundary is at  $z = 0$  [59, p. 130],

$$p(z, t) = \frac{c_m d\sigma_0 L^2 \mu}{dt} \frac{1}{2k} \left( 1 - \frac{(L-z)^2}{L^2} - \frac{32}{\pi^3} \sum_{m=0}^{\infty} \frac{(-1)^m}{(2m+1)^3} \right) \times \exp(-\Psi^2 c_f t) \cos(\Psi(L-z)). \quad (32)$$

Results of the gradual loading analysis are presented in Fig. 5. Loading rate refers to the rate of increase of applied load at the top of the column per unit time. The amount of load change per iteration ( $d\sigma_0$ ) is a function of the time step ( $dt$ ), so that a smaller load change is experienced per iteration as the time step is decreased. Time steps were chosen for A and B such that  $d\sigma_0 = (d\sigma_0/dt) \times dt$  is the same magnitude in each case. From the figure, two primary conclusions are apparent. Firstly, at the slowest loading rate (Fig. 5A) and smallest time step (and correspondingly smallest value of  $d\sigma_0$ ) there is no difference between the leapfrog approach and a simulation with additional  $p = \sigma$  iteration (inter-looping), proving the intuitive result that small explicit time steps remove the need for inter-looping. In this

case, if the time step is too large to capture the fluid-mechanical coupling, then inter-looping has little effect because more error is introduced by the fluid-mechanical couple than by the leapfrog method (evidenced by the fact that the dashed lines do not improve in accuracy over their corresponding solid lines). Secondly, a faster loading rate (Fig. 5B) results in greater error due to the leapfrog method, but lesser error due to the explicit time step size (evidenced by the relative accuracy of all three dashed lines). In other words, mechanical change (loading) is faster relative to fluid diffusion, and so the explicit time step size may be larger and still accommodate the fluid-mechanical coupling because less frequent mechanical equilibration is required to keep up with the relatively slower fluid diffusion. However, precisely because the loading rate is faster, greater error will result due to the non-iterative equilibration of stress and pressure. Therefore, a larger time step is viable, but only with inter-looping. In any case, the system may be accurately represented with the proper selection of time step and iterative method for a given rate of mechanical change, and at the slower loading rate (likely closer to those that might be seen in natural systems) the leapfrog method is sufficient provided that the explicit time step is reasonably small. For now, experimentation is required to guarantee accurate coupling.

### 7. THMC mediated aperture/permeability change

Having now examined the fluid-mechanical mechanism, we proceed to introduce further complexities that surround chemical behavior. And, because constitutive behavior in a geological system is generally non-linear, responses mediated by stress, fluid pressure, temperature, and chemical potential often require empirical examination. Notably, permeability of the system may change by orders of magnitude in response to changes in effective stress. In the following, we describe changes in permeability resulting from both stress and chemical effects, utilizing the empirical relationship proposed in [61]. That relationship is further developed herein to accommodate unloading of fracture asperities in a manner that suggests fracture gaping may occur only through mechanical means (or by thermal contribution to the stress field). Section 7.1 presents the governing loading equations as found in [61], whereas Section 7.2 illustrates an unloading construct similar to that used in [61], but where unloading is allowed to occur only through mechanical means.

#### 7.1. Loading behavior

Hydraulic aperture of a fracture under an applied effective stress,  $\sigma'$ , may be defined empirically as [3]

$$b_m = b_m^r + (b^0 - b_m^r) \exp(-\omega \sigma'), \quad (33)$$

where  $b_m$  is the hydraulic aperture (subscripted  $m$  indicating changes due solely to mechanical effects),  $b^0$  is the aperture under no mechanical stress,  $b_m^r$  is the residual aperture at maximum mechanical loading and  $\omega$  is a constant that defines the non-linear stiffness of the fracture.

The dissolution of bridging asperities may also reduce the effective aperture of the fracture. These “chemical” effects may be accommodated in the relationship for fracture aperture in a form that includes the mechanical compaction process of Eq. (33) and pressure solution-type dissolution of contacting asperities, where we have substituted  $b_m^{\max} = b^0 - b_m^r$  as the maximum possible mechanical closure [61]

$$b_{mc} = b_m^r + \{b_m^r - b_c^r + b_m^{\max} \exp(-\omega \sigma')\} \cdot \exp(-\sigma'(\beta - \chi/T)), \quad (34)$$

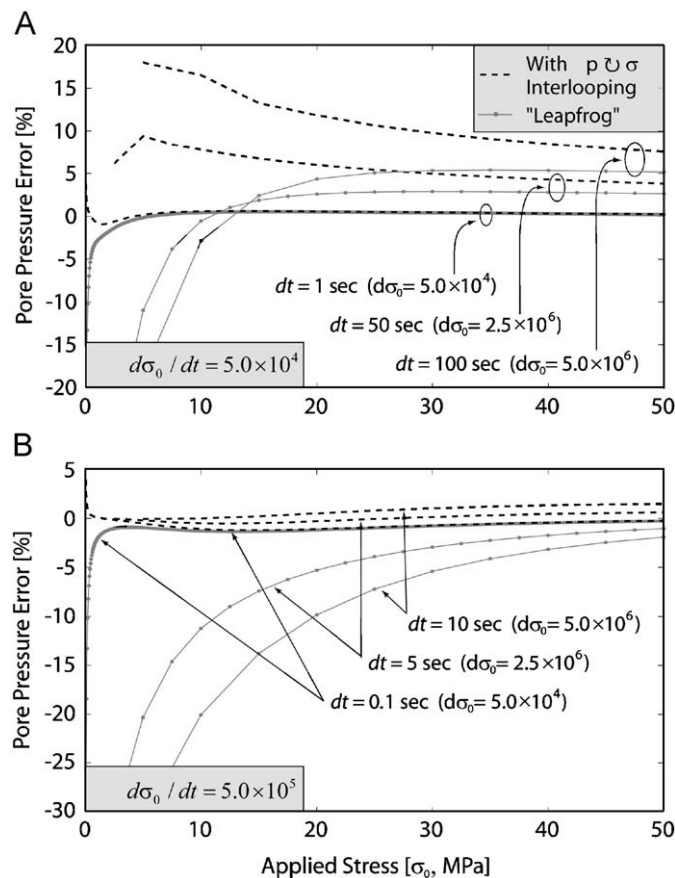


Fig. 5. Error (compared to analytical solution) in undrained pore pressure response for constant loading rate of one-dimensional vertical column for (A) slower loading rate ( $d\sigma_0/dt = 5.0 \times 10^4$ ) and (B) faster loading rate ( $d\sigma_0/dt = 5.0 \times 10^5$ ). “Leapfrog” method of simulation is solid gray line with data points. Additional inter-looping method is dashed black line.

where  $T$  is temperature and the empirical constants  $\beta$  and  $\chi$  define the chemical compaction process. The subscripted  $c$  represents changes due to chemical effects and  $b_c^r$  is the residual aperture at maximum chemical loading. Buried within these two constants (see [61]) is the critical stress [61, modified from 62,63],

$$\sigma_c = \frac{E_m(1 - T/T_m)}{4V_m}, \quad (35)$$

where  $E_m$  is the heat of fusion,  $T_m$  is the temperature of fusion, and  $V_m$  is the molar volume of the mineral comprising the fracture asperity. Dissolution of the contacting asperity will progress where the local asperity stress exceeds this critical stress that represents both the chemical and mechanical potential of the contact.

Permeability is evaluated for an orthogonal set of persistent fractures of spacing  $s$ , from the cubic law, [64,65]  $k = b^3/12s$ . Note that Eq. (34) represents equilibrium behavior, where chemically mediated changes have run to completion (i.e., it is a thermodynamic, not a kinetic relationship).

### 7.2. Unloading behavior

The above constitutive relationship governs aperture closure under conditions of thermal/mechanical loading due to the effects of mechanical deformation (Eq. (33)) and chemical alteration including mechanical deformation (Eq. (34)). If utilized in its entirety and without memory of any previous mechanical/thermal state, this represents the case of complete reversibility. However, aperture closure should not be viewed as completely reversible or irreversible, but as a mechanism that is dependent on the initial stress state and subsequent loading, as well as one that maintains memory of some attained stress magnitude and a subsequent unloading period.

For instance, subsurface storage of radioactive waste is characterized by a loading period during which temperature steadily increases and fracture apertures correspondingly decrease, followed by a period of sustained cooling towards the background state, implying a reversal of this process (fracture gaping). Alternatively, geothermal reservoirs are largely characterized by unloading behavior, where the maximum stress/temperature condition is the *in-situ* state of the fractured mass, and the injection of cooler circulation fluids causes unloading from this *in-situ* state. It is of some interest to determine the precise behavior of such an unloading period and its beginning transition.

The mechanical component of fracture closure is not a completely reversible process, but exhibits hysteresis as governed by both the elastic and plastic properties of the contacting asperities. Furthermore, while chemical behaviors may contribute to permeability *increases* through the action of thermodynamically governed dissolution, pressure solution type mechanisms as discussed above are incapable of inducing gaping of the fracture during an unloading stage (barring the inclusion of “force of crystallization” processes, pressure solution is irreversible). Therefore, it is apparent that an additional term is needed to describe the reversible portion of mechanical closure, while excluding the possibility of chemical reversibility. In this aim, we follow a procedure similar to that of Min et al. [61] to develop an unloading relationship, but maintain a reversibility that is due purely to mechanical effects.

In the simplest formulation, this need may be addressed through a mechanical recovery ratio,  $R_m$ , that governs the degree of elastic reversibility, and is defined as the ratio of the potential unloading mechanical aperture change,  $b_{m(u)}^{\max}$ , to the maximum

potential loading mechanical aperture change,  $b_m^{\max}$ , as

$$R_m = \frac{b_{m(u)}^{\max}}{b_m^{\max}}. \quad (36)$$

It is first necessary to examine the case of a mass unloaded from a state of infinite stress with the unloading version of Eq. (33)

$$b_{m(u)} = b_m^r + b_{m(u)}^{\max} \exp(-\omega\sigma'), \quad (37)$$

or, from the definition of recovery ratio

$$b_{m(u)} = b_m^r + R_m b_m^{\max} \exp(-\omega\sigma'). \quad (38)$$

However, the unloading process is dependent on the maximum loading stress (initial unloading stress). The difference in aperture between this maximum loading stress and some unloaded state is, utilizing Eq. (38),

$$\Delta b_{m(u)} = R_m b_m^{\max} \exp(-\omega\sigma_{(u)}') - R_m b_m^{\max} \exp(-\omega\sigma_{\max}'), \quad (39)$$

with the maximum (prior to unloading) effective stress  $\sigma_{\max}' > \sigma_{(u)}'$ , for any subsequent unloading effective stress,  $\sigma_{(u)}'$ . This inequality states that load cycling is not considered. The unloaded aperture is then comprised of the difference between this change and the fully loaded aperture,  $b^f$ :

$$b_{m(u)} = b^f + \Delta b_{m(u)}. \quad (40)$$

In the case of mechanical loading and unloading, the aperture at maximum loading stress,  $b^f$ , is equivalent to the final loaded aperture,  $b_m(\sigma_{\max}')$ , and so the unloading aperture is obtained by substituting Eq. (33) in Eq. (40). However, we are seeking the relationship for a fracture that has been chemically and mechanically loaded, and then unloaded along a path defined by the recoverable portion of mechanical loading. Therefore, substituting  $b^f = b_{mc}(\sigma_{\max}')$  and inserting Eq. (39) into Eq. (40) and simplifying yields

$$b_{m(u)} = b_{mc}(\sigma_{\max}') + R_m b_m^{\max} \{\exp(-\omega\sigma_{(u)}') - \exp(-\omega\sigma_{\max}')\}, \quad (41)$$

where  $b_{mc}(\sigma_{\max}')$  is Eq. (34) evaluated at  $\sigma' = \sigma_{\max}'$ . This relationship defines the aperture at a stress magnitude lower than and obtained a posteriori the fully loaded state. Eqs. (34) and (41) then fully define the loading and unloading cycle, respectively, of a fractured mass. The required empirical parameters are shown in Table 1. Parameters were obtained through a comparison with experimental results introduced in the heated block test of Terra Tek [66], where the aperture was monitored during a complete loading and unloading cycle *in-situ*, on a  $2 \times 2$  m cube of granitic gneiss subjected to stresses supplied by flatjacks with temperature alteration via borehole heaters. The original experimental results of Hardin et al. [66] are shown in Fig. 6, alongside theoretical reproduction of this behavior calculated with Eqs. (34) and (41). In the figure, loading begins at point 9 (and is isothermal for the first three data points) and continues until point 16 (non-isothermally), before being unloaded to the initial state at point 21. Hardin et al. also performed two intermediate load/unload cycles at points 13 and 16. These two intermediate cycles are not considered here, and the analytical solution is incapable of

**Table 1**  
Parameters of the permeability constitutive relationship as utilized in Fig. 6.

Parameter	Fitted value
Residual mechanical aperture, $b_m^r$ ( $\mu\text{m}$ )	6.0
Residual chemical aperture, $b_c^r$ ( $\mu\text{m}$ )	3.0
Constant in aperture relationship, $\beta$	1.00
Constant in aperture relationship, $\chi$	345
Stiffness coefficient (1/MPa)	0.375
Mechanical recovery ratio, $R_m$	0.8

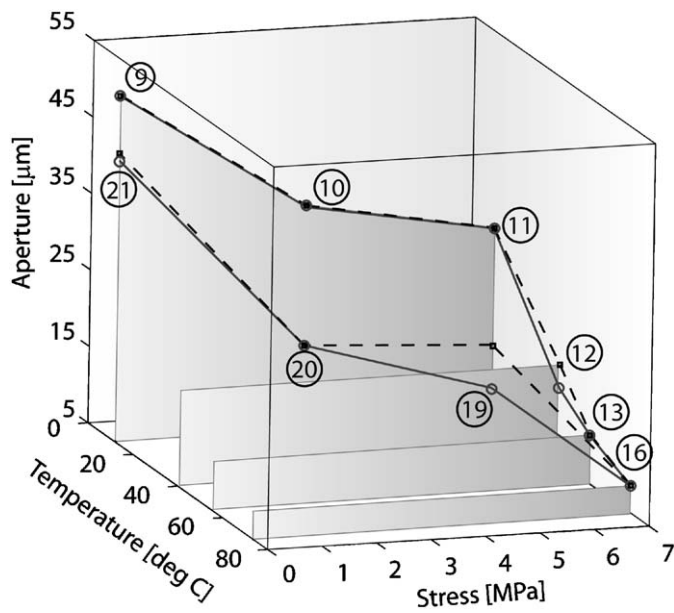


Fig. 6. Comparison of the analytical results of Eqs. (34) and (41) against experimental results of [66]. Experimental results are shown as black dashed line with solid data points. Gray solid line with hollow data points is the analytical solution. Each data point is numbered to correspond with the original data points of [66].

representing them. Agreement between the two data sets is satisfactory for the primary points of interest (intermediate loading/unloading cycling is not considered), excluding point 19, where unloading aperture cannot be reproduced with the given analytical model (which is purely mechanical and does not undergo unloading with decreasing temperature unless the stress field is altered).

### 7.3. Force of crystallization

Chemical precipitation is commonly assumed to cause a reduction in fracture aperture due to a buildup of deposited species along the fracture face. Contrary to this assumption is the concept of “force of crystallization”, dating back to 1896 with the work of Dunn [67] and 1920 with Tabor [68], with a phenomenological model presented by Weyl [8]. Force of crystallization operates analogously and inversely to pressure solution where, instead of relieving fracture stress through dissolution at asperity contacts, if the fluid is sufficiently super saturated mineral precipitation and crystal growth may exert pressure at contact points and lead to physical gapping of the fracture. Further discussion of the mechanism is available in the literature (e.g. [69–71]). While we do not, in a fundamental sense, implicitly consider the impact of this process in our model, the current logic is capable of accommodating this effect in a straightforward manner—should solution concentrations be sufficiently super saturated. The phenomenological relationship for pressure solution that we utilize is able to adequately match the laboratory studies on which it is based, all of which involve significantly under saturated fluids only.

## 8. THC mediated porosity/permeability change

Thermo-chemical induced changes in permeability may be referenced to precipitation/dissolution behaviors along the continuum fracture and matrix domains. Here, aperture changes are

caused by the addition or removal of mineral components from the walls of (at the scale of these investigations) an assumed uniform fracture face, or an isotropic porous volume fraction. This is not precisely “free face dissolution” (which implies contribution of strain energy to thermodynamic dissolution), but a purely chemically driven process governed by the rates of reaction as previously discussed. In the following, we assume that processes of this type may act independently from pressure solution over a single time step, thus enabling them to be additive over that time step. This does not indicate process independence, which would allow chemical analyses to be conducted separately of TM or of TMC without loss of accuracy. These processes are still strongly dependent on one another outside of a time step. For example, changes in permeability from pressure solution (or chemical precipitation/dissolution) will alter the flow characteristics and residence times of circulating fluids, thus modifying thermal transport. Changes in local temperature in this manner alter the stress field and modify chemical reaction rates. Modified reaction rates and residence times influence the characteristics of chemical reaction, while modified temperature and stress influence pressure solution and thermal gapping.

Changes in fracture aperture due to THC behavior are accommodated via the chemical precipitation behavior incorporated in TOUGHREACT. Addition or removal of mineral mass from the continuum system results in a change in fracture or matrix porosity within a nominal element volume, as given by the overall change in the volume of minerals present by [40,72],

$$\phi = 1 - \sum_{m=1}^N f_m^{rx} - f^u, \quad (42)$$

where  $f^{rx}$  is the volume fraction of mineral  $m$  in the surrounding rock  $v_{mineral}/v_{medium}$ , and  $f^u$  is the volume fraction of the non-reactive surrounding rock. Relations between fracture porosity and permeability are provided in the literature. One such possibility is a simple cubic relationship [34]:

$$k = k_i \left( \frac{\phi}{\phi_i} \right)^3, \quad (43)$$

where the subscript,  $i$ , refers to an initial property and  $k$ , and  $\phi$  are permeability and porosity, respectively. While several such relations may be implemented from within TOUGHREACT, it is necessary in our case to calculate permeability changes externally in order to operate multiple mechanisms simultaneously. Compatibility between the permeability change due to this behavior and that of pressure solution can be indexed to the change in fracture aperture by, as before,  $b = \sqrt[3]{12ks}$ . Aperture change via this mechanism is then assumed additive to the THMC aperture reductions associated with pressure solution driven compaction.

Several options also exist for the relationship between matrix porosity and permeability. One such possibility is the Carman-Kozeny equation [73],

$$k = k_i \frac{(1 - \phi_i)^2}{(1 - \phi)^2} \left( \frac{\phi}{\phi_i} \right)^3, \quad (44)$$

where all parameters are as previously defined, although matrix permeability is likely an insignificant contributor (in many cases) to overall system behavior.

## 9. Chemical strain and stress

Modifications in fracture aperture necessarily lead to changes in the local stress field. However, because FLAC<sup>3D</sup> uses grid point displacements to calculate strains, see Eq. (4), and does not store values of strain, no provision is available to input strains due to

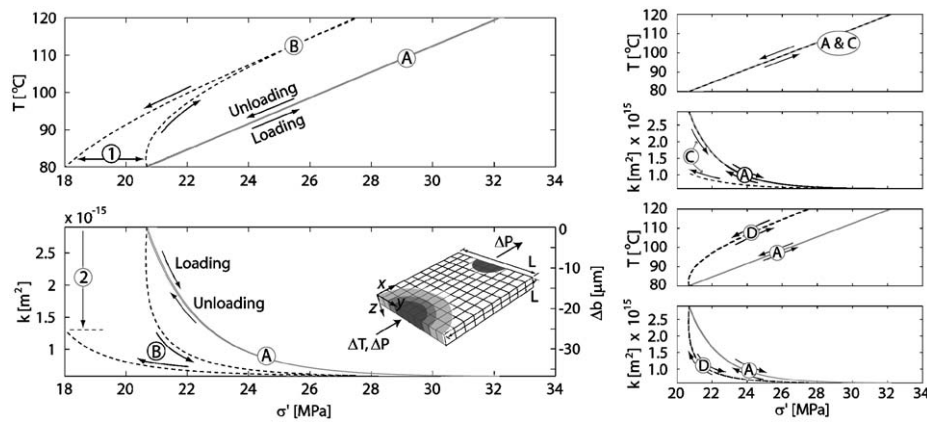


Fig. 7. Thermal loading/unloading cycle examining the effects of chemical strain. Parameters:  $E = 13 \text{ GPa}$ ,  $\nu = 0.22$ ,  $\alpha_T = 12 \times 10^{-6}/\text{K}$ .

aperture change and subsequently convert them into gridpoint displacements. An alternative method is needed.

For equally spaced orthogonal fractures, the impact of a change in aperture on local linear strain (unidirectional from a single fracture) is represented by

$$\varepsilon_{CH} = \frac{\Delta b}{s}, \quad (45)$$

where  $s$  is fracture spacing and the subscript  $CH$  refers to the “chemical strain” component of total strain owing to aperture change. In the usual manner, total strain,  $\varepsilon$ , can be spectrally decomposed into components due to mechanical,  $M$ , chemical,  $CH$ , and thermal,  $T$ , behaviors as,  $\varepsilon = \varepsilon_M + \varepsilon_T + \varepsilon_{CH}$ . Considering only thermal and chemical effects, the thermal/chemical strain is  $\varepsilon_{TC} = \varepsilon_T + A$ , where  $A$  is some constant representing the chemical portion. At incremental equilibrium we have  $\varepsilon_{TC} = \alpha_T \Delta T + A$  which, upon rearranging, becomes

$$\varepsilon_{TC} = \Delta T \left( \alpha_T + \frac{A}{\Delta T} \right), \quad (46)$$

where  $A = \Delta b/s$ . This relationship provides a method to accommodate chemical strain by altering the coefficient of thermal expansion,  $\alpha_T$ , in  $\text{FLAC}^{3D}$  at all nominal element volumes for respective aperture changes, and, as desired, maintains a non-linear dependence on temperature. However, because the function is undefined for temperature changes approaching zero, care should be taken in its application. In physical systems where aperture change, which is a strong function of the effective stress field, is dominated by thermal stress, such as geothermal systems, such strains will be tracked appropriately, but in systems that are nearly isothermal this method will be ineffective in transferring information to the mechanical system (which may or may not be necessary, as isothermal systems are unlikely to experience chemical strain to the same degree).

### 9.1. Chemical strain in cyclic loading

Chemical strain is defined here as thermo-chemo-mechanically irreversible reduction in fracture aperture that results in a relaxation of stress in the surrounding rock. As illustrated in Fig. 1, this process is proposed to be of significant importance in fractured reservoirs and replicating it one of the primary goals of THMC modeling. To examine this process, we consider the case of a liquid saturated, high temperature and pressure fractured mass subjected to a complete cycle of thermal loading and unloading (Fig. 7). The model is a pseudo three-dimensional mass (unit width in the  $z$ -direction, discretized in  $x$  and  $y$ ) with zero-displacement boundaries and initially at a uniform temperature of

$80^\circ\text{C}$ , and  $\sigma' = 20.8 \text{ MPa}$ . A high temperature ( $120^\circ\text{C}$ ) and pressure (2 MPa above *in-situ*) source is placed at one end of the geometry ( $x = 0, y = L/2$ ) with a low pressure source (2 MPa below *in-situ*) at the opposing end ( $x = L, y = L/2$ ), allowing the thermal source to translate across the geometry with the fluid pressure gradient. After thermal breakthrough to the injection temperature, the temperature source is reversed to  $80^\circ\text{C}$ , so that the mass then gradually declines to its initial temperature state. Progress is monitored at the central coordinate ( $x = L/2, y = L/2$ ), and the results of temperature and aperture change versus stress at this location are displayed.

In the figure we present four cases incorporating different assumptions of response, which may be compared to the conceptual representation of Fig. 1. Fig. 7A is the baseline case, with completely reversible permeability change (Eq. (34) only), and no feedback of this chemical strain on the stress field (Eq. (46) not used). Fig. 7B represents the case of complete permeability constitutive treatment (Eqs. (34) and (41)) and includes feedback on stress field (Eq. (46)). Fig. 7C maintains full permeability constitutive treatment (as in 7b), but this time does not include feedback on stress (Eq. (47) not used). Finally, Fig. 7D considers complete reversibility (as in 8a), but this time includes feedback on the stress field (Eq. (47)).

The non-linear dependence of aperture on the temperature/stress field is evident, as is the non-linear dependence of stress on temperature that results from the feedback of chemical strain on the stress field. Two-dominant impacts on the system, hysteretic in nature, are visible by comparing the initial, ambient system with the final, ambient system. Importantly, when the system returns to its initial state, there has been an irreversible reduction in the stress field as well as an irreversible decrease in permeability. Neither of these occurrences, intuitively operative and significant in natural systems, may be represented without the inclusion of thermal, hydrologic, mechanical, and chemical processes.

## 10. Conclusions

A coupled THMC simulator has been developed with the capability of reproducing the undrained loading behavior of a fractured rock mass. Reactive transport has been included in the model via the equilibrium behavior of aqueous species (homogeneous reactions) and through kinetic considerations of mineral precipitation and dissolution. From multi-continuum hydrogeologic analysis, multi-phase fluid behavior is coupled to the mechanical response in one continuum via dual-porosity poroelasticity and thermodynamically controlled fluid

compressibility. Permeability of the mass is followed with a new constitutive relationship representing thermal loading and unloading behavior: Closure of the fracture is controlled by thermal-elastic compaction and the dissolution of stress-concentrated asperities, while dilation occurs via thermal-hydraulic stress relaxation. Bulk permeability is also modified by the precipitation/dissolution kinetics of mineral species. The explicit coupling between THC and M behaviors is shown to reproduce the rapid response of a loaded mass. Additional couplings have also been explored, and a subsequent paper [1] examines the strength of coupling between THMC mechanisms as well as the application of this model to an EGS scenario.

Chemical strain is accommodated by the permeability constitutive relationship, and its impact on the stress field of a geologic environment is illustrated. For the first time, we present geologic scale numerical results illustrating the conceptual model that thermal loading may lead to an irreversible reduction in aperture and stress, so that the *in-situ* system may be completely altered by a cycle of loading.

## Acknowledgment

This work is the result of partial support from the US Department of Energy under Grant DOE-DE-FG36-04G014289. This support is gratefully acknowledged.

## References

- [1] Taron J, Elsworth D. Thermal-hydrologic-mechanical-chemical processes in the evolution of engineered geothermal reservoirs. *Int J Rock Mech Min Sci* 2009; this issue, doi:10.1016/j.ijrmms.2009.01.007.
- [2] Wawersik WR, Rudnicki JW. Terrestrial sequestration of CO<sub>2</sub>—an assessment of research needs. Report from invited panelist workshop, May 1997, US Dept Energy Geosci Res Prog, 1998.
- [3] Rutqvist J, Wu Y-S, Tsang C-F, et al. A modeling approach for analysis of coupled multiphase fluid flow, heat transfer, and deformation in fractured porous rock. *Int J Rock Mech Min Sci* 2002;39:429–42.
- [4] Taron J, Elsworth D, Thompson G, et al. Mechanisms for rainfall-concurrent lava dome collapses at Soufriere Hills Volcano, 2000–2002. *J Volcanol Geoth Res* 2007;160:195–209.
- [5] Nemat-Nasser S, Keer LM, Parihar KS. Unstable growth of thermally induced interacting cracks in brittle solids. *Int J Solids Struct* 1977;14:409–30.
- [6] Hunsbedt A, Kruger P, London AL. Recovery of energy from fracture-stimulated geothermal reservoirs. *J Petrol Tech* 1977;29:940–6.
- [7] Pruess K. Enhanced geothermal systems (EGS) using CO<sub>2</sub> as working fluid—a novel approach for generating renewable energy with simultaneous sequestration of carbon. *Geothermics* 2006;35(4):351–67.
- [8] Weyl PK. Pressure solution and the force of crystallization—a phenomenological theory. *J Geophys Res* 1959;64:2001–25.
- [9] Paterson MS. Nonhydrostatic thermodynamics and its geologic applications. *Rev Geophys Space Phys* 1973;11:355–89.
- [10] Revil A. Pervasive pressure-solution transfer: a poro-visco-plastic model. *Geophys Res Lett* 1999;26(2):255–8.
- [11] Elsworth D, Goodman RE. Characterization of rock fissure hydraulic conductivity using idealized wall roughness profiles. *Int J Rock Mech Min Sci* 1986;23(3):233–43.
- [12] Barton N, Bandis S, Bakhtar K. Strength, deformation and conductivity coupling of rock joints. *Int J Rock Mech Min Sci* 1985;22(3):121–40.
- [13] Rose P, Xu T, Kovac KM, et al. Chemical stimulation in near-wellbore geothermal formations: silica dissolution in the presence of calcite at high temperature and high pH. In: Proceedings of the 32nd workshop geothermal reservoir engineering, Stanford University; 2007.
- [14] Xu T, Sonnenthal E, Spycher N, et al. TOUGHREACT—A simulation program for non-isothermal multiphase reactive geochemical transport in variably saturated geologic media: applications to geothermal injectivity and CO<sub>2</sub> geological sequestration. *Comp Geosci* 2006;32:145–65.
- [15] Nami P, Schellschmidt R, Schindler M, et al. Chemical stimulation operations for reservoir development of the deep crystalline HDR/EGS system at Soultz-Souz-Forêts (France). In: Proceedings of the 32nd workshop geothermal reservoir engineering, Stanford University; 2007.
- [16] De Boer RB. On the thermodynamics of pressure solution—interaction between chemical and mechanical forces. *Geochem Cosmochem Acta* 1977;41:249–56.
- [17] Bower KM, Zvyolowski G. A numerical model for thermo-hydro-mechanical coupling in fractured rock. *Int J Rock Mech Min Sci* 1997;34(8):1201–11.
- [18] Gawin D, Schrefler BA. Thermo-hydro-mechanical analysis of partially saturated porous materials. *Eng Comput* 1996;13(7):113.
- [19] Taron J, Min K-B, Yasuhara H, et al. Numerical simulation of coupled thermo-hydro-chemo-mechanical processes through the linking of hydrothermal and solid mechanics codes. In: Proceedings of the 41st US symposium on rock mechanics, Golden, Colo, June 17–21, 2006.
- [20] Swenson D, Gosavi S, Hardeman B. Integration of poroelasticity into TOUGH2. In: Proceedings of the 29th international workshop geothermal reservoir engineering, Stanford University; 2004.
- [21] Itasca Consulting Group Inc. FLAC3D Manual: fast Lagrangian analysis of continua in 3 dimensions—version 2.0. Itasca Consulting Group Inc, Minneapolis; 1997.
- [22] Settari A. Modeling of fracture and deformation processes in oil sands. In: Proceedings of the fourth UNITAR/UNDP conference on heavy crude and tar sands, Edmonton; 1988. Paper no. 43.
- [23] Settari A, Mourits FM. Coupling of geomechanics and reservoir simulation models. *Comp Methods Adv Geomech* 1994:2151–8.
- [24] Minkoff SE, Stone CM, Bryant S, et al. Coupled fluid flow and geomechanical deformation modeling. *J Pet Sci Eng* 2003;38:37–56.
- [25] IAPWS, Industrial formulation 1997 for the thermodynamic properties of water and steam. IAPWS Release, IAPWS Secretariat, 1997: International Association for the Properties of Water and Steam.
- [26] Narasimhan TN, Witherspoon PA. An integrated finite difference method for analyzing fluid flow in porous media. *Water Resour Res* 1976;12(1):57–64.
- [27] Wilson RK, Aifantis EC. On the theory of consolidation with double porosity. *Int J Eng Sci* 1982;20(9):1009–35.
- [28] Khaled MY, Beskos DE, Aifantis EC. On the theory of consolidation with double porosity, III, A finite element formulation. *Int J Numer Anal Methods Geomech* 1984;8(2):101–23.
- [29] Cho TF, Plesha ME, Haimson BC. Continuum modelling of jointed porous rock. *Int J Numer Anal Methods Geomech* 1991;15:333–53.
- [30] Elsworth D, Bai M. Flow-deformation response of dual-porosity media. *J Geotech Eng* 1992;118(1):107–24.
- [31] Berryman JG, Wang HF. The elastic coefficients of double-porosity models for fluid transport in jointed rock. *J Geophys Res* 1995;100(12):24,611–27.
- [32] Jaeger JC, Cook NGW, Zimmerman RW. Fundamentals of rock mechanics. 4th ed. Oxford: Wiley-Blackwell; 2007.
- [33] Xu T, Pruess K. Modeling multiphase non-isothermal fluid flow and reactive geochemical transport in variably saturated fractured rocks: 1. Methodology. *Am J Sci* 2001;301:16–33.
- [34] Steefel CI, Lasaga AC. A coupled model for transport of multiple chemical species and kinetic precipitation/dissolution reactions with applications to reactive flow in single phase hydrothermal system. *Am J Sci* 1994;294:529–92.
- [35] Lasaga AC. Chemical kinetics of water-rock interactions. *J Geophys Res* 1984;89(B6):4009–25.
- [36] Lasaga AC, Soler JM, Ganor J, et al. Chemical weathering rate laws and global geochemical cycles. *Geochem Cosmochem Acta* 1994;58:2361–86.
- [37] Lasaga AC. Rate laws of chemical reactions. In: Lasaga AC, Kirkpatrick RJ, editors. Kinetics of geochemical processes, reviews in mineralogy, vol. 8. Washington: Mineral Soc Amer; 1981.
- [38] Carroll S, Mroczek E, Alai M, et al. Amorphous silica precipitation (60–120 °C): comparison of laboratory and field rates. *Geochem Cosmochem Acta* 1998;62:1379–96.
- [39] Rimstidt JD, Barnes HL. The kinetics of silica-water reactions. *Geochem Cosmochem Acta* 1980;44:1683–99.
- [40] Xu T, Sonnenthal E, Spycher N, et al. TOUGHREACT user's guide: a simulation program for non-isothermal multiphase reactive geochemical transport in variably saturated geologic media. Report LBNL-55460, Lawrence Berkeley National Laboratory, 2004.
- [41] Helgeson HC, Kirkham DH, Flowers DC. Theoretical prediction of the thermodynamic behavior of aqueous electrolytes at high pressures and temperatures: IV. Calculation of activity coefficients, osmotic coefficients, and apparent molal and standard and relative partial molal properties to 600 °C and 5 kb. *Am J Sci* 1981;281:1249–516.
- [42] Warren JE, Root PJ. The behavior of naturally fractured reservoirs. *Soc Petrol Eng J* 1963;3:245–55.
- [43] Barenblatt GI, Zheltov YP, Kochina IN. Basic concepts in the theory of seepage of homogeneous liquids in fissured rocks. *J Appl Math Mech* 1960;24:1286–303.
- [44] Pruess K, Narasimhan TN. On fluid reserves and the production of superheated steam from fractured, vapor-dominated geothermal reservoirs. *J Geophys Res* 1982;87(B11):9329–39.
- [45] Pruess K, Narasimhan TN. A practical method for modeling fluid and heat flow in fractured porous media. *Soc Petrol Eng J* 1985;25(1):14–26.
- [46] Bai M, Elsworth D, Roegiers J-C. Modeling of naturally fractured reservoirs using deformation dependent flow mechanism. *Int J Rock Mech Min Sci* 1993;30(7):1185–91.
- [47] Biot MA. Theory of propagation of elastic waves in a fluid-saturated porous solid, II. Higher frequency range. *J Acoust Soc Am* 1956;28(2):179–91.
- [48] Biot MA. General theory of three-dimensional consolidation. *J Appl Phys* 1941;12:155–64.
- [49] Biot MA. Theory of propagation of elastic waves in a fluid-saturated porous solid, I. Low-frequency range. *J Acoust Soc Am* 1956;28(2):168–78.
- [50] Biot MA. Mechanics of deformation and acoustic propagation in porous media. *J Appl Phys* 1962;33(4):1482–98.

- [51] Berryman JG, Pride SR. Models for computing geomechanical constants of double-porosity materials from the constituents' properties. *J Geophys Res* 2002;107(B3):2052.
- [52] Biot MA, Willis DG. The elastic coefficients of the theory of consolidation. *J Appl Mech* 1957;24:594–601.
- [53] Zimmerman RW, Chen G, Hadgu T, Bodvarsson GS. A numerical dual-porosity model with semi-analytical treatment of fracture/matrix flow. *Water Resour Res* 1993;29:2127–37.
- [54] Detournay E, Cheng AH-D. Fundamentals of poroelasticity. In: Hudson JA, editor. *Comprehensive rock engineering*. New York: Pergamon; 1993. p. 113–71.
- [55] Mandel J. Consolidation des sols (étude mathématique). *Geotechnique* 1953;3:287–99.
- [56] Abousleiman Y, Cheng AH-D, Cui L, et al. Mandel's problem revisited. *Geotechnique* 1996;46(2):187–95.
- [57] Rice JR, Cleary MP. Some basic stress diffusion solutions for fluid-saturated elastic porous media with compressible constituents. *Rev Geophys Space Phys* 1976;14(2):227–40.
- [58] Wang HF. *Theory of linear poroelasticity*. Princeton: Princeton University Press; 2000.
- [59] Carslaw HS, Jaeger JC. *Conduction of heat in solids*. 2nd ed. Oxford: Oxford University Press; 1959.
- [60] Geertsma J. Problems of rock mechanics in petroleum production engineering. In: *Proceedings of the first international congress rock mechanics*, vol. 1, Lisbon, 1966. p. 585–94.
- [61] Min K-B, Rutqvist J, Elsworth D. Chemically and mechanically mediated influences on the transport and mechanical characteristics of rock fractures. *Int J Rock Mech Min Sci* 2009;46(1):80–9.
- [62] Stephenson LP, Plumley WJ, Palciauskas VV. A model for sandstone compaction by grain interpenetration. *J Sediment Petrol* 1992;62:11–22.
- [63] Yasuhara H, Elsworth D, Polak A. A mechanistic model for compaction of granular aggregates moderated by pressure solution. *J Geophys Res* 2003;108(B11).
- [64] Snow DT. Anisotropic permeability of fractured media. *Water Resour Res* 1969;5(6):1273–89.
- [65] Witherspoon PA, Wang JSY, Iwai K, et al. Validity of cubic law for fluid flow in a deformable rock fracture. *Water Resour Res* 1980;16(6):1016–24.
- [66] Hardin EL, Barton N, Lingle R, Board MP, Voegelé MD. A heated flatjack test series to measure the thermomechanical and transport properties of in situ rock masses. Report ONWI-260, Columbus, Ohio: Office of Nuclear Waste Isolation; 1982.
- [67] Dunn EJ. Reports on the Bendigo Goldfield. Special reports nos. 1 and 2, Department of Mines, Victoria, Australia, 1896. p. 16.
- [68] Taber S. The mechanics of vein formation (with discussion). *Am Inst Min Met Eng Trans* 1920;61:3–41.
- [69] Wiltchko DV, Morse JW. Crystallization pressure versus “crack seal” as the mechanism for banded veins. *Geology* 2001;29(1):79–82.
- [70] Dewers T, Ortoleva P. Force of crystallization during the growth of siliceous concretions. *Geology* 1990;18:204–7.
- [71] Maliva RG, Siever R. Diagenetic replacement controlled by force of crystallization. *Geology* 1988;16:688–91.
- [72] Lichtner PC. Continuum formulation of multicomponent-multiphase reactive transport. In: Lichtner PC, Steefel CI, Oelkers EH, editors. *Reactive transport in porous media*. Washington, DC: Mineral Soc Amer; 1996.
- [73] Bear J. *Dynamics of fluids in porous media*. New York: Elsevier; 1972.